Control of neoclassical tearing modes

M.Maraschek

Max-Planck-Institut für Plasmaphysik

E-mail: Maraschek@ipp.mpg.de

Abstract. Neoclassically driven tearing modes (NTM) are a major problem for tokamaks operating in a conventional ELMy H-mode scenario. Depending on the mode numbers these pressure driven perturbations cause a mild reduction of the maximum achievable $\beta_N = \beta_t/(\frac{I_p}{aB_t})$ before the onset of the NTM, or can even lead to disruptions at low edge safety factor, q_{95}. A control of this type of modes in high β_N plasmas is therefore of vital interest for magnetically confined fusion plasmas. The control consists of two major approaches, namely the control of the excitation of these modes and the removal, or at least mitigation, of these modes, once an excitation could not be avoided. For both routes examples will be given and the applicability of these approaches to ITER will be discussed.

1. Introduction

In terms of overall performance, neoclassical tearing modes (NTMs) are limiting the maximum achievable toroidal normalized pressure $\beta_t = \langle p \rangle/(B_t^2/2\mu_0)$ (see footnote to equation (1)) and hence also the global normalized $\beta_N = \beta_t/(I_p/aB_t)$. Here I_p denotes the plasma current in MA, B_t the vacuum toroidal field in T, a the minor radius of the plasma in m and $\langle p \rangle$ the volume averaged total pressure. The onset of an NTM leads to a significant degradation in confinement, but does not have a hard limit in β_N, as one would expect for an ideal MHD-limit. (3/2)-NTMs with poloidal and toroidal mode number of m=3 and n=2 lead to a confinement loss of up to 20%. Especially at low q_{95} (2/1)-NTMs lead to an even greater loss in confinement and ultimately can lead to disruptions. The role of low collisionality $\bar{\nu}_{ii}$ for an increased propability for (2/1)-NTMs and disruptions is rather complicated and multiple explanations are discussed in literature. The achievable β_N at the mode's onset can be increased by optimizing the discharge scenario, as for example shown in [1, 2]. The most commonly applied theory describing the behaviour of the NTMs is based on a generalized Rutherford equation including the additional neoclassical term, which drives the island. This main driving force originates the local bootstrap current $j_{bs}(r_{res})$ at the resonant surface. It is governed by the local pressure gradient ∇p, which is mainly proportional to the local poloidal normalized pressure $\beta_p(r_{res}) = \langle p(r_{res}) \rangle/(\langle B_p(r_{res})^2 \rangle/2\mu_0)$ (see footnote to equation (1)) at the resonant surface of the mode.

Based on this theory a stabilization or removal of an excited NTM is possible by local current drive and heating at the resonant surface. This has been shown experimentally on various experiments and will a major part of this paper. After a brief description of the

underlying physics for NTM removal and avoidance, a discussion of the available tools for this target is followed by an overview over the most important experimental steps for the stabilization of NTMs and their overall avoidance. If the modes can be neither avoided nor suppressed, the question, if one could mitigate or live with existing NTMs while maintaining good plasma performance is addressed. Finally, a discussion of the transferability and applicability for ITER will be discussed, which is followed by the summary highlighting open questions in this area.

2. Description of the NTM physics and their suppression or avoidance

2.1. Generalized Rutherford equation with ECRH current drive

The generalized Rutherford equation with additional terms due to the neoclassical driving term, the polarization current term and the $\chi_\perp/\chi_\parallel$-term provides a widely accepted description of neoclassically driven tearing modes [3, 4] ‡

$$\begin{aligned}\frac{\tau_{res}}{r_{res}}\frac{dW}{dt} &= r_{res}\Delta'(W) \\ &+ r_{res}\beta_p\left(a_2\sqrt{\varepsilon}\frac{L_q}{L_p}\frac{W}{W^2+W_0^2} - a_3\frac{r_{res}}{R_0^2}\frac{L_q^2}{L_p}\frac{1}{\sqrt{W^2+0.2W_{d,e}^2}}\right. \\ &\quad \left. -a_4 g(\varepsilon,\nu_{ii},\omega_e^*,m)\left(\rho_{pi}\frac{L_q}{L_p}\right)^2\frac{1}{W^3}\right) \\ &- c_{stab}16\sqrt{\pi}\mu_0 r_{res}L_q\frac{j_{ECCD}}{B_{pol}}d_{dep}\frac{\eta_{ECCD}}{W^2}\end{aligned} \tag{1}$$

Besides the classical tearing mode stability parameter Δ' resulting from the equilibrium current gradient at the resonant surface r_{res} [5], additional destabilizing and stabilizing terms are included. The terms with the coefficients a_2, a_3, a_4 describe the neoclassical bootstrap drive with the finite perpendicular to parallel heat conductivity correction ($\chi_\perp/\chi_\parallel$-correction), which is included in W_0 [6], the stabilizing Glasser term introduced by the helical component of Pfirsch-Schlüter currents induced by toroidicity and shaping of the poloidal cross-section [7, 8, 9, 10] and the stabilizing polarization currents induced by the island rotation within the background ion fluid [11]. The gradient length for all quantities is calculated according to $L_\alpha = \alpha/\nabla\alpha$, with $\nabla = \frac{d}{dr}$, where r measured in meters is the minor radius of the flux surface on the low field side of the plasma. Hence, in this approximation the gradients are described in 1/m and $[L_\alpha] = \mathrm{m}$ holds. The local poloidal ion gyro radius ρ_{pi}^* at the resonant surface is defined as $\rho_{pi}^*(r_{res}) = \rho_{pi}/a = \frac{\sqrt{2m_i kT_i(r_{res})}}{e\langle B_p(r_{res})\rangle}/a$, where a is the minor radius of the plasma in the

‡ r_{res}: minor radius of the resonant surface of the considered mode (distance from the magnetic axis to the intersection of a horizontal line from the axis to the low field side with the flux surface), τ_{res}: resistive time scale on resonant surface; L_p, L_q: pressure gradient and q-gradient scale length; a_i: numerical constants of the order of unity; W: island width; $\varepsilon = r_{res}/R_0$: inverse aspect ratio of the resonant surface; R_0: major radius of the geometric axis of the resonant surface; ρ_{pi}: poloidal ion gyro radius at the resonant surface; $\beta_p(r_{res}) = \frac{\langle p(r_{res})\rangle}{\langle B_p(r_{res})^2\rangle/2\mu_0}$: flux surface averaged poloidal β_p; $\beta_t = \frac{\langle p\rangle}{B_t^2/(2\mu_0)}$ volume averaged toroidal β, with B_t being the vacuum toroidal magnetic field; d_{dep}: deposition width at $1/e$ of the maximum of a Gaussian radial deposition profile of the externally driven ECCD current.

horizontal plane of the magnetic axis. The poloidal magnetic field $\langle B_p(r_{res})\rangle$ is defined as the averaged poloidal field $B_p(r_{res},\theta)$ on the resonant surface.

In the above shown form of the generalized Rutherford equation (1) the polarization current term (a_4-term) diverges for $W \to 0$. A full kinetic treatment [12, 13, 14] shows that finite-orbit effects weaken the impact of the polarization current on the island stability, although a complete description of the related physics is still lacking. As done in equation (1) in [4], the divergence of the polarization contribution can be removed in the corresponding term by changing $\sim 1/W^3$ into a term of the form $\sim W/(W^4+W_{d,pol}^4)$.

It is important to note, that the density gradient ∇n and the temperature gradient ∇T have a differently weighted impact on the variation of the local bootstrap current $j_{bs}(r_{res})$, as applied in [15]. The corrected pressure gradient length according to [3] results in

$$\frac{1}{L_p^{corr}} \approx \frac{1}{1+\alpha}\cdot\left(\frac{1}{L_T}+\alpha\cdot\frac{1}{L_n}\right), \text{ with: } \alpha = 2.5. \tag{2}$$

The weighting factor $\alpha = 2.5$ has been experimentally fitted. The $T\cdot\nabla n$ term thus contributes stronger to the bootstrap current than the $n\cdot\nabla T$ term. As shown in [16], the onset and marginal β scalings and the time history of an NTM could only be achieved by including this distinction between the influence from the temperature and the density gradient.

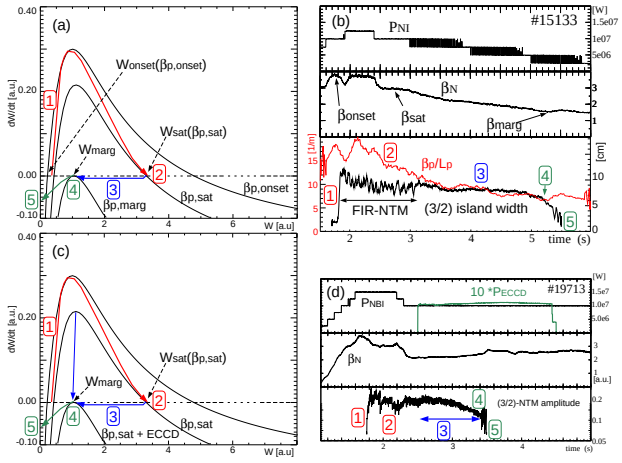

Figure 1. (a) Stability diagram for a naturally occurring NTM in terms of the island growth rate dW/dt as function of the island width W. Characteristic points in terms of β_p and W are marked. (b) Corresponding time traces of a natural NTM with the important time points marked. In the modified stability diagram (c) the effect of the application of additional current drive at the resonant surface is shown and (d) shows the corresponding time trace for a removal with additional Electron Cyclotron Current Drive (ECCD, see the text for more details).

In figure 1 the characteristic values of an NTM are indicated (a) in the stability diagram and (b) the time traces of an experiment measuring the so-called marginal $\beta_{p,marg}$ of the mode. The stability diagram represents the solution of equation (1) for different values of the plasma pressure represented by the local $\beta_p(r_{res})$. At the maximum $\beta_p = \beta_{p,onset}$ two solutions of the equation with $dW/dt = 0$ exist. The right solution represents the saturated island size W_{sat} and the left solution minimal seed island size W_{seed}. For an NTM to get excited, this W_{seed} has

to be provided on the resonant surface by an external perturbation, such as a sawtooth (point 1 in figure 1 (a) and (b)). The flattening of the pressure profile over this initial island reduces the bootstrap current locally within this so-called seed island. For conventional monotonic q-profiles, this defect current acts as the major drive of the NTM. During the subsequent growth of the NTM to its saturated size $W_{sat}(\beta_{p,sat})$, the mode degrades the confinement. The normalized pressure drops until a new equilibrium is reached at a lower $\beta_{p,sat}$ (point 2 in figure 1). At the highest β_p values a (3/2)-NTM can occur as so-called FIR-NTM, described in the next paragraph. When the external heating power is continuously reduced, the island size $W_{sat}(\beta_p)$ follows mainly the local $\frac{L_q}{L_p^{corr}}\beta_p$ values [4, 16] ($W_{sat}(\beta_p) \sim \frac{L_q}{L_p^{corr}}\beta_p$) and continuously shrinks (points 2,3,4 in figure 1 (a) and (b)). This can be approximated with $W_{sat}(\beta_p) \sim \frac{1}{L_p^{corr}}\beta_p \sim \beta_p$. The value of β_p, for which W_{sat} and W_{seed} become one identical solution, is defined as the marginal β_p, i.e. $\beta_{p,marg}$. This single solution is defined as the marginal island width $W_{marg} := W_{sat}(\beta_{p,marg}) = W_{seed}(\beta_{p,marg})$. When β_p is reduced below $\beta_{p,marg}$ the island decays away ($dW/dt < 0$ for all $\beta_p < \beta_{p,marg}$, at point 5 in figure 1 (a) and (b)). The dependence $W_{sat}(\beta_p) \sim \beta_p$ no longer holds for $\beta_p < \beta_{p,marg}$. When the NTM has disappeared, β_p can rise again due to the recovered confinement. It can even exceed again $\beta_{p,marg}$ until the next external trigger may excite again a new NTM. In the shown example β_p even rises while the heating power is still ramped down. Exact formulas for these characteristic quantities can be found in [17], [18], [4] and [19]. In [19] the quantities are used in a way that they can be applied directly for predictions towards ITER and the the NTM stabilization there. The stabilization process by local Electron Cyclotron Current Drive (ECCD) in figure 1 (c) and (d) will be explained in the next section.

For higher local β_p-values, just after the onset of the (3/2)-NTM, a phase with frequent interruptions of the (3/2)-NTM growth can be observed, which is caused by nonlinear coupling to a (4/3) and a (1/1)-mode. This behaviour can not be described with equation (1), but requires additional non-linear calculations [20]. This coupling reduces the (3/2)-NTM amplitude on a very short time scale. Thus for a repetition time of these rapid amplitude drops smaller than the NTM growth time ($\tau_{FIR-drop} < \tau_{growth}$), the average island width W gets reduced and does no longer follow the local β_p-values, as shown in [4, 16]. This behaviour is described as **F**requently **I**nterupted **R**egime, FIR-NTM [21, 22, 20]. At lower β_p values the (4/3) mode bursts remain stable, i.e. the FIR phase disappears and the (3/2) mode follows the local β_p values. The threshold for this FIR behaviour is described by an empirically determined critical β_N at the mode's onset, $\beta_{N,onset} \geq \beta_{N,FIR} = 2.3$.

2.2. Stabilization of excited NTMs

The dominant driving term for the NTM is the lack of the bootstrap current within the island, as the pressure profile is flattened and therefore the bootstrap current is reduced. For the unperturbed bootstrap current $j_{bs} \sim \nabla p/\langle B_p \rangle$ holds. This opens the possibility to directly remove an NTM by locally replacing the missing current [23, 18]. by external means, such as local Electron Cyclotron Current Drive (ECCD, see chapter 3). In the stability diagram and the time traces this process is illustrated in figure 1 (c) and (d). The external local current

drive is turned on, while the plasma is in a stationary equilibrium at $\beta_{p,sat}$ with an island size of $W_{sat}(\beta_{p,sat})$ (point 2 in figure 1 (c) and (d)). The additional ECCD term (c_{stab}-term) in the generalized Rutherford equation (1) now shifts the stability curve, while keeping the high $\beta_{p,sat}$, to a lower a value in dW/dt. Within the c_{stab}-term, d_{dep} denotes the deposition width at $1/e$ of the maximum of the Gaussian radial profile of the externally driven ECCD current $j_{ECCD}(r) = j_{ECCD,0} \cdot e^{-((r-r_{dep})/(2d_{dep}))^2}$. Throughout this paper always this definition has been used. The right solution W_{sat} is reduced and the island shrinks with increasing size of the c_{stab}-term (points 2, 3 and 4 in figure 1 (c) and (d)). Having reached $W_{sat}(\beta_{p,sat}, ECCD) = W_{marg}$, the island decays away, as in the previous case when β_p had been reduced (point 5 in figure 1 (a) and (b)). In the example shown in figure 1 (d) the magnetic field is slowly varied until the resonant surface is hit correctly. This variation is slowly increasing the c_{stab}-term. After the removal of the NTM, β rises again, as desired.

As done in [24], the additional term with the factor c_{stab} describing the effect of local current drive with Electron Cyclotron Current Drive (ECCD) at the resonant surface has been included. The remaining ECCD independent terms have been summarized in only one experimentally fitted parameter c_{sat}. With this simplification of the Rutherford equation ASDEX Upgrade and JT-60U data of stabilization experiments have been used to calculate a these fit parameters to $c_{sat} = 0.81 \pm 0.13$ and $c_{stab} = 0.68 \pm 0.22$ (as used in equation (1)). The resulting predictions for ITER will discussed in section 8.

A crucial quantity for the stabilization is the ratio between the maximum externally driven current density $j_{cd,max}$ at the start of the stabilization process and the defect current density of the missing bootstrap current at the saturated phase $\eta_{NTM} := j_{cd}/j_{bs}$. The requirement for ITER has been estimated based on experimental data both for the (3/2) and the (2/1)-NTM to $\eta_{NTM} \geq 1.2$ for large β at the onset compared to the marginal β_{marg}, i.e. $\beta_N >> \beta_{N,marg}$ [25]. This translates for the island size W into $W_{sat} \approx W_{onset} >> W_{marg}$. From JT-60U and DIII-D different requirements on η_{NTM} for ITER have been reported based on experimental data [26, 27, 28]. The smaller requirement on η_{NTM} might be due to the consideration of an island size just above the marginal island size, i.e. only $W_{onset} > W_{marg}$holds. Only an moderately higher β above β_{marg} has been applied at the modes onset. Also depending on the full deposition width $2d_{dep}$ compared to the marginal island width W_{marg}, a variation of the requirements might be needed [29, 30, 19]

Recent works have derived an analytical expression for η_{NTM} without the need for empirically fitted coefficients in the generalized Rutherford equation [31]. This calculation takes advantage of the fact, that most of the terms included in η_{NTM} originate from the same generic term for a helical current perturbation. The two cases of a dominating transport term ($\chi_\parallel/\chi_\perp$-term) or for a dominating polarization current term are included by distinct formulas for η_{NTM}^{tra} and η_{NTM}^{pol}. The remaining experimentally free parameters are the saturated island size W_{sat} and the marginal island size W_{marg}. The classical tearing mode stability parameter Δ' has been approximated in terms of the fully saturated island size W_{sat} without any additional ECRH or ECCD applied (c_{stab}-term = 0, $j_{ECCD} = 0$) as $\Delta' := -\Delta'_{BS}(W = W_{sat})$. For this determination also $dW/dt = 0$ has been used (stationary, i.e. saturated island). The remaining terms have been taken as $\Delta'_{BS}(W = W_{sat})$ and have been calculated from the profiles. Both

the island size and the deposition width of the ECCD have been normalized to the physically relevant marginal island size W_{marg}, i.e. $\bar{W} := W/W_{marg}$ and $\bar{W}_{dep} := (2d_{dep})/W_{marg}$ Also these results will be discussed in section 8 for a prediction for ITER.

2.3. Avoidance of the excitation of NTMs

In order to avoid the excitation of NTMs in the first place, there are different options, which are implemented in present day devices. Considering the main drive of the NTM, the missing bootstrap current, a local reduction of the unperturbed equilibrium bootstrap current $j_{bs}(q = m/n)$ should reduce the maximum reachable island size and in particular the excitability of the mode. Considering the different influence of the density gradient and the temperature gradient on the bootstrap current, a reduction of the local density gradient $\nabla n_e(q = m/n)$ at the resonant surface reduces the propability for an NTM excitation. This can be done without any local current drive, as it relies on the profiles, which can be achieved within the considered discharge scenario.

The second approach for avoiding NTMs, lies in the avoidance of MHD, which provided the trigger for NTMs, i.e. avoid the seed island. This concentrates mainly on the avoidance of sawteeth and fishbones at the $q = 1$ surface. A variation of the stability of the m=1/n=1 activity at the q=1 surface is the key for this task.

An alternative way is the tailoring of the global shape of the q-profile with, typically broader, external current drive. Here, the resonant surface with $q = m/n$ is completely avoided in the plasma and hence the corresponding (m/n)-NTM can not be excited. This idea can not only be applied for the avoidance of the NTM itself, but also for the avoidance of the triggering MHD, namely the avoidance of sawteeth and fishbones by avoiding the $q = 1$ surface.

3. Relevant systems for controlling and detecting NTMs

Both for the stabilization of existing NTMs, as well as for their avoidance a local modification of MHD stability is required. Replacing the missing bootstrap current at a specific resonant surface is one possibility. The most widely used tool at present experiments is the Electron Cyclotron Resonance Heating (ECRH) and in particular the Electron Cyclotron Current Drive (ECCD).

3.1. Electron Cyclotron Resonance Heating and Current Drive (ECRH / ECCD)

The key advantages of this technique are narrow localization in the order of centimetres in the radial direction, which typically is smaller than the saturated island width W_{sat} of a (3/2)-NTM and a (2/1)-NTM. In the vertical direction the deposition width is defined by the focus of the propagating beam, which is of the same order. Moreover, the deposition radius of ECRH and ECCD in terms of the minor radius can be easily controlled with a steerable mirror system. Via a modulation of the gyrotron voltage the emitted power can be modulated in the range of the rotation frequency of an NTM, i.e. in the 10 kHz to 20 kHz range in present experiments. For ITER, this frequency is expected to be in the order of 2 - 3 kHz, due to the lower expected

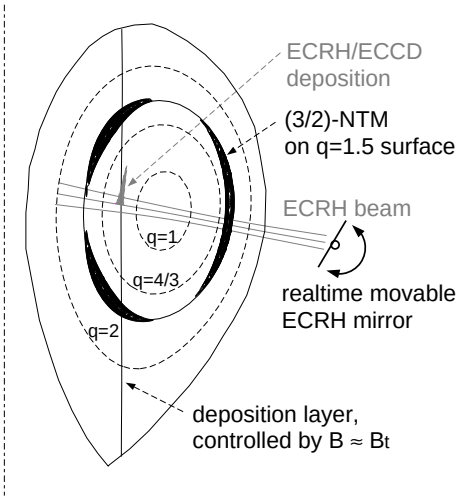

Figure 2. Scheme for controlling the ECRH/ECCD deposition for a stabilization of a (3/2)-NTMs. The localization of the ECCD is primarily governed by the total magnetic field $|B|$, which can be approximated by the main toroidal field B_t. The detailed localization is governed by the poloidal angle of the ECRH/ECCD launching mirror.

plasma rotation. The modulation is mandatory, when the full ECCD deposition width $2d_{dep}$ is larger than the marginal island width W_{marg} [32].

3.1.1. Control of the ECCD deposition on a resonant surface The deposition location of the ECRH wave propagating through the plasma (see figure 2) is mainly governed by the total magnetic field $B = \sqrt{B_t^2 + B_r^2 + B_\theta^2}$, including the response of the plasma itself. As this field is dominated by the toroidal field component B_t, the deposition is mainly occurring at a fixed major radius R, as $B_t \approx B_0 \cdot \frac{R_0}{R}$ holds. When the beam propagates perpendicular to a density gradient, the beam propagation is modified and typically bent away from the region of high density. Therefore, in general the deposition has to be calculated by a beam/ray-tracing code, such as TORBEAM [33, 34, 35] or TORRAY-GA [36]. The deposition on a specific resonant surface, such as the $q = 3/2, 2/1, 4/3$ surface, can be achieved with a variation of the poloidal angle of the launching mirror. The toroidal angle (perpendicular to the drawing plane in figure 2) to lowest order controls the amount of driven current.

Before dynamically steerable mirrors were available, the global plasma position (e.g. at DIII-D) or the magnetic field B_t has been controlled (e.g. at ASDEX Upgrade and JT-60U), in order to ensure the ECCD deposition hits the relevant resonant surface. For the first time, a direct control of the ECRH mirror [37] and a feedback control [38] has been used at JT-60U.

3.1.2. Control of the ECCD phase in O-point of the NTM The above consideration assumed a rotating island with an island width W larger than the deposition width $2d_{dep}$ of the ECCD ($W > 2d_{dep}$). When the island becomes smaller during the stabilization process, it eventually gets smaller than the deposition ($W < 2d_{dep}$). An increasing amount of current is driven outside the islands separatrix and the efficiency of the stabilization is reduced. When the

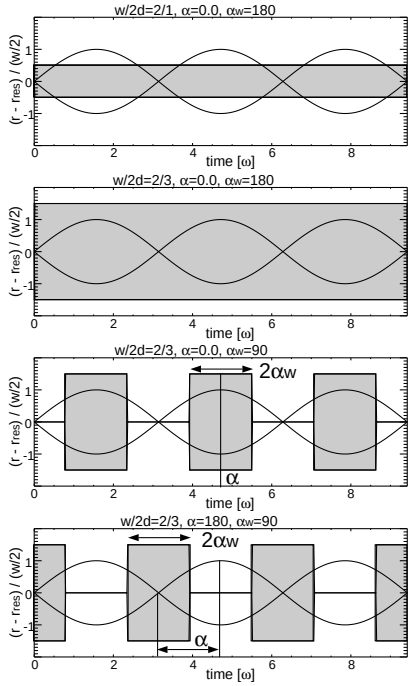

Figure 3. Sketch of a (3/2) island propagating in front of one gyrotron launchers for full period of the mode. The deposition phase is indicated by the shaded area. From top to bottom: Narrow deposition $2d_{dep}$ compared to the island width W ($W/2d_{dep} > 1$), broad deposition ($W/2d_{dep} < 1$), favourable broad deposition with ECCD modulation in the O-point, unfavourable broad deposition with ECCD modulation in the X-point.

marginal island size W_{marg} is also smaller than the deposition width ($W = W_{marg} < 2d_{dep}$), the mode can no longer be stabilized [39, 32]. In this case the ECCD needs to be modulated to deposit power only inside the island's separatrix close to the O-point, as it has been shown theoretically and experimentally [32, 40]. These situations are indicated in figure 3.

By simply modulating the ECCD power, typically 50% of the gyrotron power is not used. The unused power is cooled in the gyrotrons system and hence lost for the stabilization scheme. Therefore, techniques have been developed to switch the gyrotron power between different beam paths. The different paths now reach the plasma via different wave guides and different launching mirrors in order to follow the O-point of the island in space. These so-called **FA**st **DI**rectional **S**witches (FADIS) [41, 42] have been successfully developed and tested at the ECRH setup at W7-X [43]. Here high power switching with up to 20 kHz for a pulse duration of 10 s has been achieved.

Both for simple modulation and for the use of multiple beam paths the phase of the ECCD deposition location and the phase of the island have to be carefully mapped onto each other via an equilibrium reconstruction, as indicated in figure 4.

3.2. Ion Cyclotron Resonance Heating (ICRH)

In principle also ICRH has the capability of driving current in a plasma. Due to the applied frequencies and hence wavelengths and the size of the antennas of such systems, a narrow

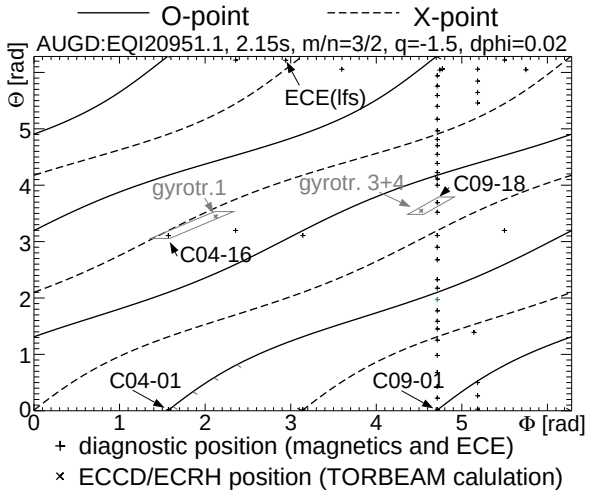

Figure 4. Localization of the ECCD depositions (tilted crosses) with respect to the magnetic field lines of the X (dashed lines) and the O-point (solid lines) on the resonant surface according to an equilibrium reconstruction (adapted figure 5 from [32]). Individual magnetic pickup (crosses) coils in this example are located close the deposition location in 3d space, which has been calculated with TORBEAM. The ECE diagnostic measurement position is also marked as a reference point for the mode detection.

localization, comparable to the ECRH systems, is not possible. The deposition widths in R and Z direction are much larger and the resonant surfaces could not be hit locally enough in experiments at JET. Due to the deposition distribution at experiments at JET it was not possible to perform such experiments, as a significant power fraction would have reached the first wall [44].

The more important role of the ICRH lies in tailoring the sawtooth stability via a modification of the fast particle distribution. The interaction between such fast ion populations and the ideal internal kink mode at the $q = 1$ surface is considered as an important explanation for a modification of the sawtooth behaviour [45] and is supported by recent JET data [46]. The global current drive capabilities might be a tool for controlling the current profile for NTM avoidance scenarios.

3.3. Lower hybrid current drive (LHCD)

At COMPASS-D successful stabilization of NTMs with Lower Hybrid Current Drive (LHCD) could be achieved [47, 48]. In these experiments it is reported, that the main effect for the stabilization of a (2/1)-NTM comes from the variation of the current gradient at the resonant surface, i.e. a reduction of the $r_{res}\Delta'(W)$-term with roughly 10% additional LHCD power compared to the background heating.

At JET a range of experiments has been performed with LHCD. In these experiments no successful removal of an existing NTM could be achieved. The radial localization of the driven current could not a priori be controlled and was typically too broad for this purpose.

The effect of LHCD on the current profile can be exploited in a more global way as it has been done at JT-60U for q-profile tailoring, as described later in detail. The absence of a

$q = m/n$ surface obviously avoids the excitation of a (m/n)-NTM. Newer results from JT-60U even show the suppression of existing (2/1)-NTMs [26].

3.4. External coils for repositioning of locked modes

If an NTM, in particular a (2/1)-NTM, grows to a sufficiently large size, it eventually locks to the intrinsic error field in a characteristic postion. In such a situation the mode stops rotating and remains in a fixed position and eventually stops the entire plasma rotation. The plasma can no longer be described as a 2d equilibrium, but has to be treated as a full 3d equilibrium containing the (2/1) locked mode as a perturbation. Especially for low q_{95} this situation often leads to a disruption (see figure 9a).

Applying ECCD on the resonant surface with a locked mode, is more complicated. The ECCD deposition spots have to be aligned with the O-point. The adjustment of the deposition above and below the midplane allows for some adjustment, but does not in general assure pure current drive in the O-point. The proper alignment between the O-point of the island and the ECCD deposition can be analyzed via a mapping with the help of the plasma equilibrium, as indicated in figure 4.

A possible way to resolve this problem lies in the modification of the locking position of the mode itself. This can be achieved by controlling the intrinsic error field of the experiment. At DIII-D the total error field can be modified by additional internal coils [49]. This system can generate a static or a rotating error field with a toroidal mode number of $n \leq 3$. JET has $n \leq 2$ error field correction. ASDEX Upgrade has started operating an set of internal coils in 2011 with $n \leq 2$, which will be extended in the 2012 campaign to $n \leq 4$ [50, 51, 52]. With such artificial internal perturbation at DIII-D the locking position of a mode could be controlled.

3.5. Relevant measurements for detecting NTMs

All of the described tools are actuators for an integrated NTM controller. Such a controller, however, must get information from the plasma about the existence, the poloidal and toroidal mode number m and n and in particular the radial location of the mode with respect to the minor radius. For modulated injection in the O-point of the island, also the phase of the mode is required. It has to be noted, that obviously all these signals have to be provided in realtime and communicated to the control system, on which the NTM controller is running on.

For the detection of the existence of NTMs, most importantly the (3/2) and the (2/1) NTM, magnetic pick-up coils are being most widely used as the obvious choices. A integrated and weighted sum of Mirnov coil (B_θ-measurement) provides, depending on the weights, most easily signals for the magnetic perturbation amplitude at the plasma edge of a mode with a specific m and n number (spatial Fourier filtering). Applying a set of thresholds on this signal gives the information when a certain (m/n)-NTM gets excited and when it has been successfully removed again.

The radial localization of the mode with respect to the flux surface is most easily and directly possible with a local temperature measurement with the ECE diagnostic [53, 54]. The FFT amplitude and phase profile reveal the mode localization (phase jump of π at the

resonant surface) and the island width directly. At various experiments also a correlation analysis within the ECE data alone and in connection with the magnetic signal has been suggested and implemented [55, 56, 57, 58] and references therein. The ECE diagnostic also provides a direct measurement of the deposition of the ECRH itself using power modulation. This might remove the requirement of a raytracing code calculating the ECCD deposition in realtime.

For a proper mapping of the measurements from the ECE a reliable and well defined equilibrium is needed (for example in [59]) Ideally this would be based on a direct current density measurement. The Motional Stark Effect (MSE) measurement at least provides directly measured pitch angles of the local magnetic field (for example in [60]), which helps to constrain the equilibrium reconstruction.

For calculating the expected deposition of the ECRH / ECCD system a raytracing code has to be operated in realtime. For this also electron density and temperature profiles have to be available. Such systems are presently indeed available at multiple experiments. As soon as the ECCD is really switched on, the ECE measurement provides a complementary information, which might also serve as a correction for the calculated values of the deposition.

A possible way around the mapping procedures is the so-called in-line (or oblique or line-of-sight) ECE. In this case an additional ECE diagnostic is embedded in the mirror system measuring the emitted light from the plasma in the vicinity of the deposition location of the ECRH system directly. Any mapping between the different diagnostic system via the plasma equilibrium becomes unnecessary. Such a system has been implemented and successfully used for mode stabilization at TEXTOR [61, 62] and DIII-D [40].

In the future also a soft X-ray (SXR) diagnostic may provide additional information on the radial mode localization. However, this is more complicated, as the SXR diagnostic measures integrated line of sight measurements from multiple cameras. Even without a full tomography, a correlation analysis with the magnetic measurements might provide complementary information to the NTM controller.

4. Stabilization of excited NTMs

Over the last years on many experiments, which have an ECRH / ECCD system available, experiments have been performed, which have shown that both (3/2) and (2/1)-NTMs in high β_N discharges can be reliably removed. In this section an overview of these experiments will be given.

4.1. Removal of rotating (3/2) and (2/1)-NTMs

First experiments for a removal of rotating (3/2)-NTMs were performed with a modulated injection, targeting for the O-point [63] (figure 5). A variation of the relative phases between O-point and X-point showed, that only with O-point phasing a reduction of the island size by 40% is possible with 4%-8% additional ECCD power compared to the background NBI power. The radial location of the ECCD deposition has been varied on a shot-to-shot basis by

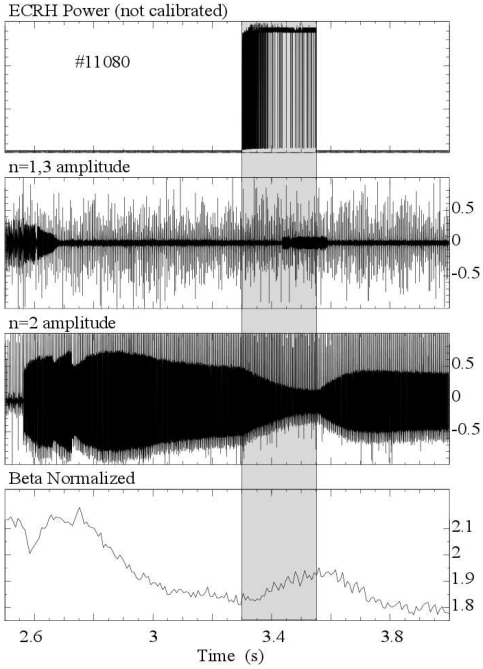

Figure 5. First clear reduction of an (3/2)-NTM with modulated ECCD, which becomes unmodulated at sufficiently small island sizes, due to a failure of the trigger system for the modulation. (figure 2 from [63] The unmodulated phase, which is technically much easier to handle, is almost as effective.

varying the main toroidal field B_t. About 5% of β_N could be recovered for the first time by such a scheme. In these initial attempts it turned out, that unmodulated co-ECCD was almost as efficient as modulated ECCD. Most of the following experiments have been performed only with unmodulated ECCD. This could be done, as for most of the experiments a deposition width $2d_{dep}$ smaller than the marginal island width W_{marg} could be easily achieved. The different behaviour for O and X-point phasing could be well understood with the help of an MHD code which includes self-consistently the local bootstrap current [64, 65, 66].

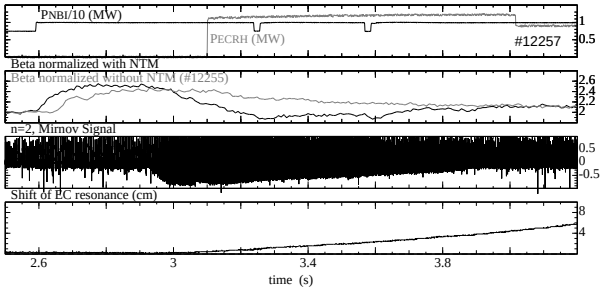

Figure 6. Complete stabilization of a (3/2)-NTM (black traces in box 2, #12257) in comparison with a discharge without the excitation of an NTM (grey traces in box 2, #12255), due to a missing sawtooth trigger. The same β_N values could be reached after the NTM removal compared to the reference case. (adapted figure 1 from [67])

Later experiments with an increased amount of unmodulated co-ECCD power showed for

the first time the possibility of a complete removal of a (3/2)-NTM [67]. With typically 10% additional co-ECCD power it is possible to recover the discharge during a pre-programmed magnetic field ramp, finally reaching a β_N, which is identical to a discharge without any NTMs (figure 6). The global β_N in these experiments slowly decreases due to the applied magnetic field ramp.

Consequently the next step is the stabilization of the more dangerous (2/1)-NTM. The complete stabilization of a (2/1)-NTM has been achieved for the first time at DIII-D [27]. In these experiments both feedforward programmed ramps of the toroidal field B_t (figure 7), as well as the SEARCH-AND-SUPPRESS algorithm [55] has been used with the toroidal magnetic field as actuator to hit the resonant surface As sensor for the size of the NTM the amplitude of an integrated Mirnov coil ($\int \frac{dB_\Theta}{dt} dt$) has been used.

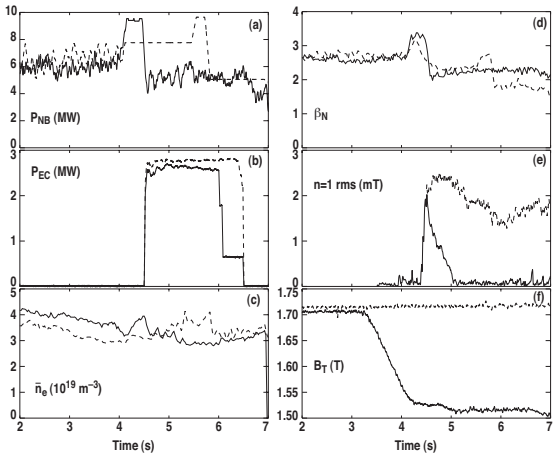

Figure 7. Complete stabilization of a (2/1)-NTM at DIII-D (figure 9 from [27]). The boxes show the applied NBI power P_{NB}, the achieved β_N, the applied ECCD power P_{EC}, the $n = 1$ magnetic field perturbation from the NTM, the line averaged density $\bar{n}_e$ and the magnetic field B_t. The dashed traces represent a discharge with constant magnetic field, where the ECCD was not hitting the $q = 2$ surface and the NTM could not be removed. The solid traces represent a discharge, where the magnetic field B_t has been used as an actuator from the control system for depositing the ECCD on the $q = 2$ surface. In this case the NTM could be completely removed in less than a second.

At ASDEX Upgrade, the (2/1)-NTM has been stabilized without feedback control, again with a feedforward programmed magnetic field ramp [68]. The ECCD was in this case applied to a locked (2/1)-NTM, which for $q_{95} \geq 3.3$ typically does not lead to disruptions [69]. The phasing could not be actively controlled with respect to the locking position of the mode, as ASDEX Upgrade at that time was not equipped with internal coils for generating a dedicated perturbation field. The gyrotron system and the mirror position was located in a position, where the typical locking position allowed to hit the O-point.

In COMPASS-D a complete stabilization of a (2/1)-NTM with LHCD has been shown [47, 48]. As mentioned above, the main effect for the stabilization of the (2/1)-NTM was done via the current gradient at the resonant surface, i.e. a reduction of the $r_{res}\Delta'(W)$-term. Roughly 10% additional LHCD power was needed to achieve this removal. Experiments

at JT-60U were performed from a very early stage on with mechanically steerable launcher mirrors [37] and a feedback control to keep the deposition at the resonant surface [38].

4.2. Experiments steering the ECCD phase in the islands O-point

It has been experimentally shown at ASDEX Upgrade, that when the island becomes norrower than the ECCD deposition width, unmodulated ECCD is not able to reduce the island bellow its marginal width W_{marg} and hence not able to completely remove the island for the same ECCD power applied (see for example figure 8a taken from figure 4 from [32]) [32, 63]. The ECCD has been deliberately made broader compared to the technical constraints by increasing the toroidal launching angle. The ECCD has been modulated by varying the emitted gyrotron power by using an $n = 2$ filtered Mirnov coil ($dB_\theta/dt_{n=2}$) signal for the modulation control. With an additional voltage comparator, which has been implemented in the hardware, a binary signal has been generated for that purpose. With such a setup and the correct phasing with the ECCD in the O-point, the mode could again be completely removed again (see figure 8 b). A dedicated phase scan of the deposition has shown, that the X-point localized injection is only slightly worse compared to the unmodulated case.

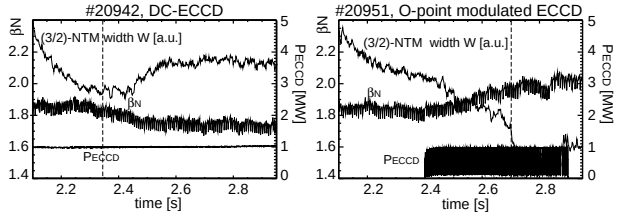

Figure 8. Comparison between two identical discharges with unmodulated (a) and modulated (b) broad ECCD deposition. Only the B_t-ramp has been slightly adapted to match the resonance condition between ECCD and the mode. The vertical dashed lines indicate the time when the resonance is reached and the minimum island size W_{min} is reached. Only in the modulated case W_{min} gets reduced below the marginal island size W_{marg} and the mode disappears (figure 4 from [32]

At DIII-D at this point another trigger scheme has been used [40]. An oblique ECE diagnostic embedded in the mirror system of the ECRH heating system has been used to provide a trigger signal for the modulation of the ECCD itself. This has the advantage, that no 3 dimensional mapping of the problem, as indicated in figure 4 is needed. The increased efficiency has been quantified by a reduction of 10% of the peak ECCD power and a reduction of 30% of the time averaged ECCD power to completely remove the island.

Subsequent experiments at JT-60U also performed a modulated stabilization of the more dangerous (2/1)-NTM [26]. The source for the modulation in these experiments was also a magnetic pickup coil. It could be shown, that the island decay rate of the (2/1)-NTM is about 1/3 faster compared to the unmodulated case. A dedicated scan of the relative phase clearly shows the advantageous effect of deposition in the O-point. In addition, the detrimental effect of modulated deposition in the X-point could be shown.

4.3. Locked (2/1)-NTMs before disruptions - disruption avoidance

Typically at low q_{95} and at low collisionality $\bar{\nu}_{ii}$ [70] (2/1)-NTMs get excited. However, the role of the collisionality is rather complex. The polarization current term in equation (1) is one possible candidate. The interplay between n_e and T_e-profile and its impact on the bootstrap current (see equation (2)) and hence the NTM drive is another possible explanation. The particle transport, which is obviously influenced by the collisionality, might create a modified overall presssure and q-profiles at low collisionality. In such plasma conditions, a (2/1)-NTM can lead to mode locking, which eventually stops the entire plasma rotation. The perturbation field of the mode interacts with the vessel wall or with intrinsic error fields and brakes the plasma rotation. Finally this situation can lead to a disruption, as shown in the example in figure 9a.

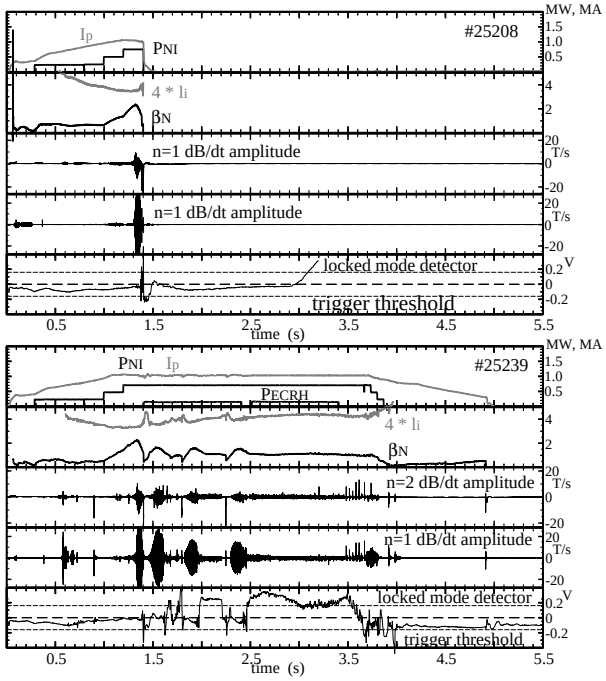

Figure 9. (a) High β_N discharge with low $q_{95} = 3.8$ resulting in a disruption due to the locking of a (2/1)-NTM. From top to bottom the plasma current I_p and the injected beam power P_{NBI}, the achieved β_N and the ideal limit $4l_i$, the $dB_{pol}/dt(n = 2)$ signal of a set of Mirnov coils, the $dB_{pol}/dt(n = 1)$ signal of a set of Mirnov coils and the locked mode signal with its trigger threshold is shown. The locked mode signal is clearly above the preprogrammed trigger threshold for ECRH application. (b) In an identical discharge the trigger has been used to switch on the ECRH twice for a preprogrammed phase of 1s. The (2/1)-NTM unlocks several times due to its reduction in size and does no longer lead to a disruption. (adapted figure 1 from [71])

Experiments on ASDEX Upgrade have shown, that local heating in the vicinity of the resonant $q = 2$ surface, is able to unlock the (2/1)-NTM and avoid the disruption (figure 9b) [72, 71]. Surprisingly pure heating with ECRH has been an order of magnitude more effective compared to the application of ECCD in recent experiments. DIII-D experiments on the other hand have shown a clear beneficial effect of ECCD over pure ECRH [40, 73]. From the usual

understanding one would expect, that current drive, such as ECCD, should be even more effective compared to pure heating.

In the DIII-D experiments additionally a variation of the phasing between the applied ECCD and the phase of the island has been performed. In this part of the experiment a clear beneficial effect of the deposition in the O-point has been observed. Only in this case the locked mode could be removed completely removed while remaining in the locked position. The X-point phasing is comparable to the case without applying ECRH or ECCD at all. In both cases, natural unmitigated disruption and X-point phased ECCD, the discharge disrupts approximately at the same time. The locking position of the mode has been controlled by an externally applied artificial error field [73, 74].

The disagreement on the effect of ECCD versus ECRH is an issue that needs to be addressed in the future, and could possibly be explained by the fact that the toroidal phase of locking position was controlled by an auxiliary error field in the DIII-D experiments. This allowed the ECCD current to be driven deliberately in the O-point, where it is known to have the most stabilizing effect. At ASDEX Upgrade such a control of the mode position is planed in the future. At present the phasing of the ECCD relative to the mode position could not be controlled at ASDEX Upgrade.

The possibility of a complete disruption avoidance with local ECCD / ECRH, in particular in high β_N-discharges, is very important for safe tokamak operation. Within a global control scheme the ECCD/ECRH based disruption avoidance will play an important role, as it is not only restricted to high β_N scenarios. For most disruption types a locking (2/1) mode occurs, which is often a classically driven tearing mode. For other disruptive paths alternative avoidance or at least mitigation schemes will have to be included in a control system. This discussion however goes beyond the scope of the present paper.

5. Avoidance of the excitation of NTMs

5.1. Preemptive ECCD at resonant surface(s)

At JT-60U local ECCD has been applied at the resonant surface before the onset of a (3/2)-NTM [75, 76]. In these experiments the onset of the (3/2)-NTM could be significantly delayed. For the same amount of applied ECCD power before the excitation of the mode, the saturated island size remained smaller compared to the case when the ECCD is applied after the mode has reached its naturally saturated size (figure 10 and left part of figure 11). The accuracy requirements on the exact radial localization of the ECCD with respect of the resonant surface $q = m/n$ are identical as in the usual application of the ECCD after the NTM onset (right part of figure 11). The (3/2)-NTM could be reliably avoided, if the variation of the deposition radius Δr_{dep} was in the order of the half width of the deposition width $2d_{dep}$ itself ($\Delta r_{dep} \approx 2d_{dep}$). The radial deposition has been controlled during the NTM lifetime via a realtime controlled steering of the launching mirror system, while the starting value was based on experience from previous discharges.

At DIII-D similar experiments could completely avoid the excitation of a (3/2)-NTM

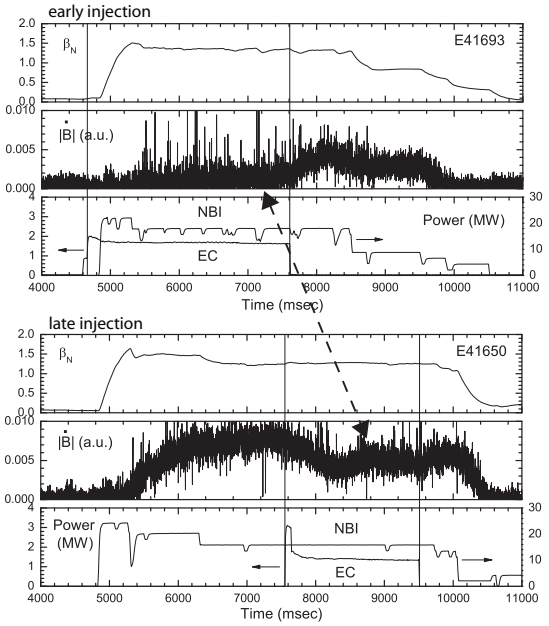

Figure 10. Time traces for a comparison between early and late ECCD injection from JT-60U (taken from figure 1 from [75]). With early ECCD (before modes onset) the saturated island size never becomes as large as in the late ECCD case. In this case the ECCD deposition is kept fixed at the pre-calculated $q = 3/2$ surface. In the case of late ECCD the deposition is controlled via a steerable mirror on the resonant surface, where the mode is located.

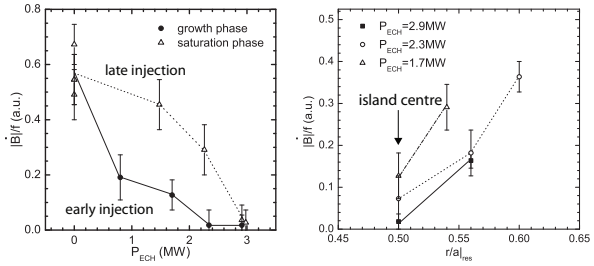

Figure 11. Laft part: For early ECCD the maximum island size remains more than a factor of 2 smaller. Right part: The radial localization remains a critical issue, both for early and late ECCD application (taken from figure 2a, 3a from [75]).

by preemptive ECCD at the resonant surface. As shown in figure 12, the excitation could be completely avoided while β_N is ramped up to $4l_i$, the assumed ideal limit. Sawteeth and fishbones occur, which would normally trigger an NTM [77]. In these experiments the ECCD deposition has been controlled also via the launching mirror system using a full realtime equilibrium reconstruction for estimating the resonant surface before the mode excitation.

For the (2/1)-NTM a complete avoidance of the mode could also be achieved in the presence of an already excited (3/2)-NTM [78], as shown in figure 13. In this experiment instead of moving the mirrors the toroidal magnetic field B_t has been used as the actuator from the control system.

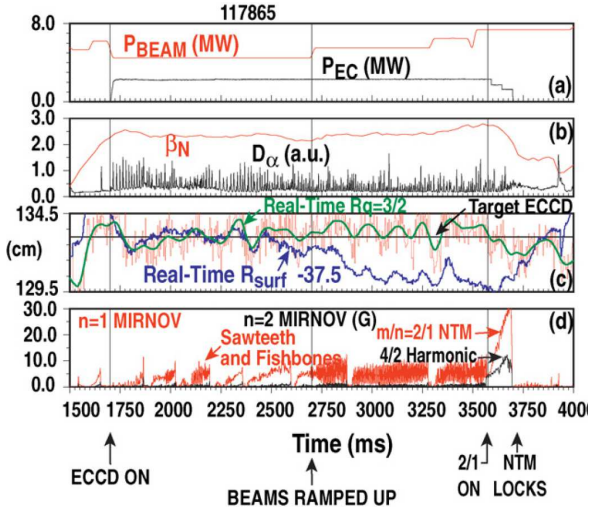

Figure 12. Complete prevention of the excitation of a (3/2)-NTM in the presence of preemptive ECCD at the $q = 3/2$ surface (taken from figure 2 from [77]). During the preemptive ECCD phase only sawteeth and fishbones are observed, which would typically trigger a (3/2)-NTM in such a scenario.

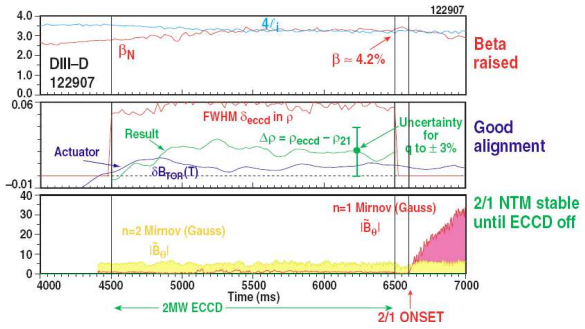

Figure 13. Prevention of the additional excitation of a (2/1)-NTM in the presence of an already excited (3/2)-NTM in the presence of preemptive ECCD at the $q = 2$ surface (adapted figure 5 from [78]). The mode location has been tracked via a realtime equilibrium information. The actuator for controlling the radial position has been the main toroidal magnetic field B_t.

5.2. Profile tailoring with wave heating

As indicated above the main drive for an NTM is the pressure gradient at the resonant surface. In particular, the dominant part of the pressure gradient is the local density gradient [3, 79]. A local reduction of the density gradient dn_e/dr should therefore be beneficial for a reduced saturated island size W_{sat}. The excitation of an NTM by a large enough trigger should be less likely.

With a centrally flattened n_e profile and hence reduced bootstrap drive the excitation of NTMs could be avoided entirely [80, 15]. In figure 14 an example is shown, where in the presence of central ICRH the excitation of a (3/2)-NTM appears at a significantly higher β_N.

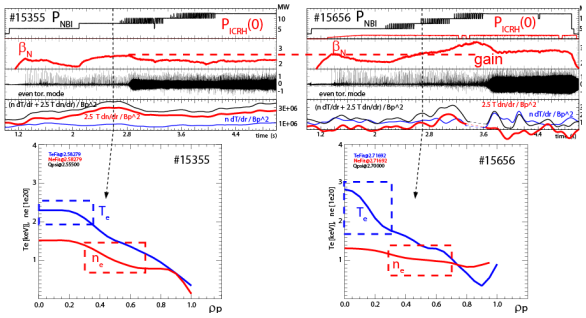

Figure 14. Two otherwise identical discharges without (left) and with central (right) electron heating via ICRH are compared. From top to bottom the applied heating power, the achieved β_N, the even magnetic amplitude $dB_{pol}(n=2)/dt$, the total corrected pressure gradient and its parts from ∇n_e and ∇T_e are shown. At the bottom the n_e and T_e profiles at the indicated time points are shown for the two cases.

With central electron heating, in this case via ICRH, an increased outward particle transport can be observed depending on the value of the collisionality. This can be understood in terms of an interplay between Trapped Electron Modes (TEM) and Ion Temperature Gradient driven modes (ITG), which is theoretically described [81] and experimentally observed [82].

However, as already indicated such approaches are only possible in the appropriate collisionality range (see [81] for details). The central electron heating in a fusion reactor will be supplied by the α-particle heating. Whether the appropriate collisionality range is reached for such an effect, is an open question and has to be shown experimentally in the future. The available electron heating by ECRH might be insufficient, to overcome the dominant self heating provided by the plasma, in order to make this a possible control tool. A dedicated reduction of the peaking of the central density might also be detrimental for fusion power generation in a later fusion device.

Another approach lies in the combined tailoring of the q-profile and the overall pressure profile, which has been performed at JT-60U [83]. The current profile has been modified by LHCD in combination with off axis NBI heating, in such a way that both the $q = 3/2$ and the $q = 2/1$ are radially located in a region with an reduced pressure gradient. At $q_{95} = 4.5$ a stationary high $\beta_N \approx 2.4$ could be achieved for a duration of 5.8s ($\approx 2.5\tau_R$). An extension of this profile tailoring was leading to a scenario with extremely low $q_{95} \approx 2.2$ at $\beta_N \approx 3$ stationary for $\approx 6s$ (see figure 15). By drastically reducing the plasma cross section still at full plasma current I_p and toroidal field B_t, an extremely low $q_{95} \approx 2.2$ could be achieved. Both the $q = 3/2$ and $q = 2$ surface have been shifted into region with $\rho_{pol} \geq 0.7$, where $\rho_{pol} = \sqrt{(\psi - \psi_{axis})/(\psi_{separatrix} - \psi_{axis})}$ denotes the normalized poloidal flux ψ as radial coordinate. Due to the off-axis NBI heating a broad pressure profile has been established, such that the relevant resonant surfaces are in a region with reduced pressure. The central q-profile becomes flat and no sawteeth or fishbones are observed, i.e. no triggering MHD is available. All these ingredients are considered to contribute to this NTM free discharge.

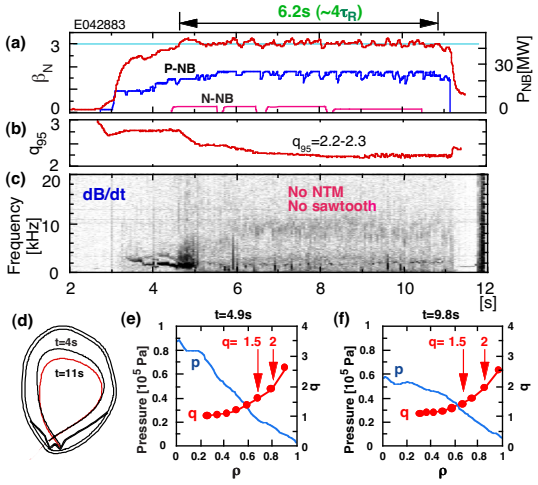

Figure 15. Time traces of the achieved stationary β_N and the applied heating powers (a) for a high β_N, low q_{95} discharge at JT-60U (Reprint with permission from figure 5 from [83], Copyright 2005, American Institute of Physics.). The q_{95} (b) is lower by a shrinking of the plasma cross section (d). During the low $q_{95} \approx 2.2$ phase no MHD is observed (c). The pressure and q-profiles are adjusted in a way that the $q = 3/2$ and $q = 2$ surface are located radially in a region ($\rho_{pol} \geq 0.7$) with reduced pressure (e,f).

5.3. Current profile control with LHCD with excited NTM

At JT-60U experiments with LHCD were performed with an entirely different approach. The LHCD was used to establish a current profile, which does not support the excitation of an NTM at all [84]. Obviously the absence of a certain resonant surface with $q = m/n$, removes the possibility for a (m/n)-NTM to occur at all. In the reported experiments the minimal q-value, q_{min} has been controlled via off-axis LHCD in feedback operation after the NTM onset. As soon as q_{min} rises above $q = 2/1$, the existing (2/1)-NTM disappears and the now removed confinement degradation allows for a recovery of β_N (see figure 16).

5.4. Avoidance of NTM triggering MHD

Another actively investigated approach for the NTM avoidance, is the removal of MHD instabilities in the plasma, which typically trigger NTMs.

At JET experiments with ICRH and ICCD around the $q = 1$ surface have been performed [1]. It is possible to stabilize sawteeth, i.e. create large and less frequent sawteeth (large τ_{st} between two subsequent sawteeth), as well to destabilize them and create smaller and more frequent sawteeth (small τ_{st}). With large τ_{st} and large sawtooth crashes NTMs could be triggered at very low β_N values, whereas for small τ_{st} and small sawteeth NTMs could be avoided almost reaching the ideal limit before triggering an NTM during a ramp of the external NBI heating power. These experiments have been interpreted later in more detail in terms of interaction between fast ion population and the ideal internal kink mode at the $q = 1$ surface [45] and are supported by recent experimental data from JET [46].

At TCV experiments with local ECRH and co and counter-ECCD have been performed

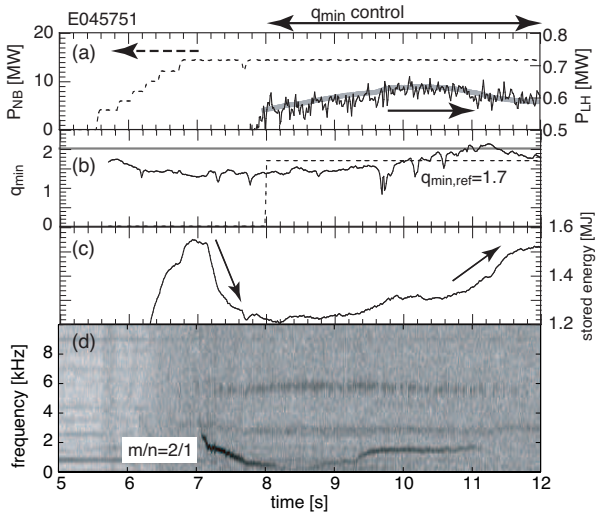

Figure 16. Removal of a still rotating (2/1)-NTM through current profile control via off-axis LHCD (figure 6 from [84]). The additional LHCD heating (a), which is feedback controlled, increases the q_{min} (b) until it greater than 2. As soon as $q_{min} > 2$ holds, the (2/1)-NTM disappears (d) and the stored energy (c) can recover.

in order to modify the sawtooth period and hence the size of the crashes. Both experimentally and in particular theoretically the effect of heating and current drive could be disentangled. The importance of the magnetic shear around the $q = 1$ surface has been shown [85]. These considerations have been performed in terms of the linear resistive stability threshold of the internal kink.

Based on a complete radial scan of the deposition of pure ECRH heating, co-ECCD and counter-ECCD on a shot-by-shot basis, a clear characterization of the sawtooth behaviour as function of the deposition radius has been achieved at ASDEX Upgrade [86, 87]. The local current drive around the $q = 1$ surface leads to a variation of the q-profile and hence the gradient $\nabla q(q = 1)$ at the resonant surface. The co-ECCD with its accompanying reduced resistivity due to the heating effect has been most effective here. Pure ECRH heating showed similar results, whereas the counter-ECCD case was less effective. For current drive with ECCD the heating effect is always present, which has a similar effect as co-ECCD due to the increased inductively driven current when the plasma becomes locally hotter. The variation of the sawtooth stability could be explained in terms of a de / stabilization of sawteeth by an increase / decrease of q' at the $q = 1$ surface. Both a decrease of the sawtooth size with decreasing τ_{st}, as well as an increase of the sawtooth size with increasing τ_{st}, even up to a complete avoidance of sawteeth could be achieved by a variation of q'. This scheme has been used to avoid sawtooth triggered NTMs in a high β_N discharge during the full pulse length of the co-ECCD [88]. Only after the ECCD around the $q = 1$ surface was switched off, the sawteeth revert back to their normal size and a (3/2)-NTM is promptly triggered. This scheme for sawtooth tailoring needs an exact control of the deposition with respect to the $q = 1$ surface. Therefore a feedback controlled ECCD deposition is mandatory, but not as critical as for the NTM removal itself.

Recent TCV [89] and modeling results [90] have shown two new approaches, namely sawtooth pacing and locking respectively. A combination of sawtooth detection via central Soft X-ray measurements and realtime control of the feedback controlled ECCD power in the vicinity of the $q = 1$ surface allows a control of the occurrence of the next sawtooth crash, i.e. apply sawtooth pacing [89]. Such a scheme significantly reduces the required ECCD power, as the power is no longer required continuously. New simulation results propose a new scheme, sawtooth locking, where the sawtooth cycle could be phase locked to an externally applied modulated ECCD deposition [90]. In this case no feedback control is required. Note that the latter has been confirmed and demonstrated in TCV [91]. For both approaches models have been discussed explaining the observed behaviour of the sawteeth.

At ASDEX Upgrade a comparison between different NBI sources with different injection angles and deposition profiles has been done. A significant variation of the individual sawtooth size and the sawtooth period have been observed [87]. For the most tangential and off-axis deposition large sawteeth with large τ_{st} (stabilization) has been observed, whereas for more radial and central injection small sawteeth with small τ_{st} (destabilization) has been observed. More recent experiments have used a control of the depositions radius of an individual NBI source for producing large sawteeth in combination with ICRH heating [92]. The detailed distribution of NBI generated fast ions around the close $q = 1$ surface plays a crucial role there. The application of ECCD is able to destabilize these artificially stabilized large sawteeth again and consequently remove the large sawteeth, which potentially trigger NTMs [93]. An comprehensive overview over the control of sawteeth is given in [94].

It must be noted however, that in the absence of sawteeth and fishbones NTMs can be triggered at higher β_N values also by other MHD events, such as ELMs at the plasma edge. At even higher values of β_N, NTMs can also be initiated without any obvious trigger, and grow "out of the noise" at an early state of the discharge. For these consideration the following inequality holds $\beta_{onset}(\text{sawtooth}) < \beta_{onset}(\text{fishbone}) < \beta_{onset}(\text{ELM}) < \beta_{onset}(\text{trigger-less})$ [95].

6. Effect and mitigation of unavoidable NTMs

There might be cases when neither avoidance nor stabilization of excited NTMs is possible. This might be due to a lack of available ECRH power for avoidance or complete removal. The question arises, whether it is still possible to partially recover the confinement loss due to the NTM or whether it is possible to design scenarios where the NTM induced confinement loss is tolerable.

6.1. Triggering the FIR regime

As described in section 2.1, for high enough $\beta_{N,onset} \geq 2.3$ the FIR regime with a nonlinear coupling between a (3/2)-NTM, an ideal, so called (4/3) infernal mode and a (1/1) mode can be reached. In this FIR regime the confinement loss due to a (3/2)-NTM is reduced from the usually expected 20% down to a level of $\approx 10\%$ (see figure 17) [21, 22, 20].

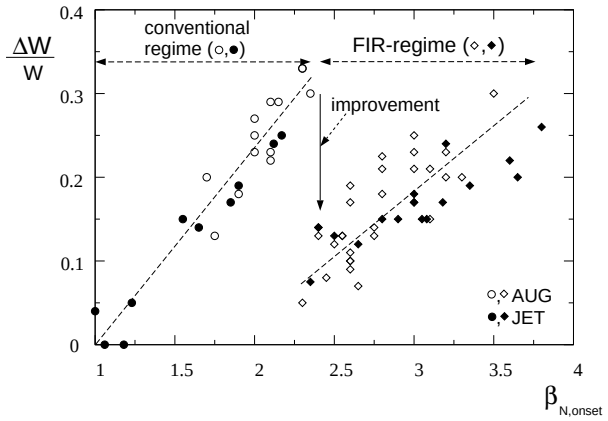

Figure 17. Confinement loss $\Delta W/W_{onset}$ due to an existing (3/2)-NTM as function of the β_N value at the NTM onset for a combined data set from ASDEX Upgrade and JET. (adapted figure 4 from [20]). Open symbols denote ASDEX Upgrade data, full symbols JET data. The circles below the critical threshold $\beta_N \approx 2.3$ represent the conventional occurrence of NTMs, whereas the diamonds above $\beta_N \approx 2.3$ represent the FIR regime, with a reduced loss $\Delta W/W_{onset}$.

With the application of co-ECCD or counter-ECCD, for this purpose at the $q = 4/3$ surface, it is possible to destabilize or stabilize the (4/3)-mode externally (see figure 18). With the stabilization, the entry into this beneficial regime can be suppressed, whereas with destabilization of the (4/3)-mode, access can be gained already at lower β_N values (see figure 8 and 9 in [20] and figure 18). Although higher confinement values are accessable with such a modification of the NTM behaviour, the applicability for a reactor is not straight forward. The complete removal of a (3/2)-NTM and in particular of a (2/1)-NTM is still the most attractive approach, as it promises the largest gain in confinement and β_N. However, the access to the FIR-regime should be considered as a possible mitigation choice.

6.2. Beneficial effect of NTMs in improved H-mode / hybrid scenario

In the conventional ELMy H-mode with a monotonic q-profile and $q_0 < 1$, (3/2)-NTMs generate the confinement loss discussed above. However, in the so-called improved H-mode or hybrid scenario the presence of a (4/3)-NTM or a (3/2)-NTM only has negligible impact on the confinement [96, 97, 98]. In this scenario one typically reaches a flat central q-profile with $q_0 \approx 1$. This current profile is clamped by the presence of these modes. Alternatively, stationary (1/1)-fishbone activity can occur, which also maintains a rather flat current profile. For the hybrid scenario at DIII-D [99, 100, 101] and JET [102] findings are fully consistent with this picture. Similar MHD behaviour and impact on the confinement is reported. It has been shown, that also in such scenarios a complete stabilization of (3/2)-NTMs is possible together with an improvement in confinement [103]. The ultimate limiting MHD phenomenon for the improved H-mode or hybrid scenario is the excitation of (2/1)-NTMs. The formation of such scenarios is left to references, as this goes beyond the scope of this paper.

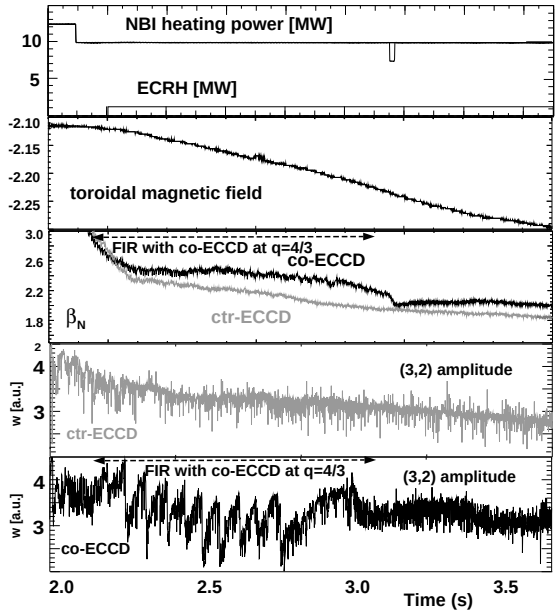

Figure 18. Artificial suppression or triggering of the FIR-regime by local counter (grey traces) or co-ECCD (black traces) at the $q = 4/3$ surface in two otherwise identical discharges. From top to bottom the time traces show the identically applied NBI and ECCD power, the applied magnetic field ramp, the varying β_N traces, the island width of the (3/2)-NTM in the non-FIR and in the FIR case respectively. The applied B_t-ramp is used to scan for the resonance with the (4/3)-surface. In the presence of the (4/3)-mode the FIR-regime, with its characteristic amplitude drops, is accessable in the case of co-ECCD (black traces). An increase of almost 20% in β_N can be achieved in comparison to the non FIR-regime with counter-ECCD (grey traces) ($t \approx 2.3s - 2.8s$ in 3^{rd} and the 5^{th} box, the relevant time interval is indicated for the co-ECCD traces; adapted figure 8 from [20]).

7. Combining the sensors and actuators into a control scheme

All the above described detection and intervention concepts have to be combined to an integrated scheme for controlling the occurrence, the mitigation or ultimately the removal of NTMs.

These approaches contain tailoring of the q-profile, the j_{bs}-profiles and hence mainly the n_e-profiles, in order to remove the relevant resonant surface or the generic drive for NTMs, respectively. However, this might be impossible under the constraints of an energy producing high performance plasma, as a high central pressure is needed for a high fusion power output. Avoidance of the triggering MHD is a possibility, which mainly consists of the control of (1/1) activity at the $q = 1$ surface. For both avoidance schemes central or slightly off-axis current drive is the appropriate method.

For removal of unavoidable NTMs the local current drive with ECCD seems to be an appropriate choice. For small islands the current has to be modulated, in order to deposit only power in the O-point. In this approach at least two independent current drive tools, such two gyrotrons and two mirrors, for the (3/2) and the (2/1)-NTM respectively, have to be in stand-by and aim at the resonant surfaces without firing. As soon as an NTMs appears they have to

fire until the NTM gets stabilized again, while tracking and correcting for the radial location of the mode.

The analysis and the decision process for this has to be implemented as a real-time algorithm dealing with fast realtime signals and has to control actions of the external heating systems. Presently such kind of algorithms are being implemented or are already in parts in operation on multiple experiments. However, most of these approaches presently do not contain the complete set of actions in a fully automatic way. Such a complete integration is still an important task for the future, in order to gain operation experience for ITER.

At DIII-D a sophisticated system is implemented, which was using the so-called SEARCH-AND-SUPPRESS algorithm [55]. This algorithm was originally using the magnetic field and the radial plasma position as the main actuator. Later this scheme has been adapted to also control the poloidal mirror position of the ECRH launchers. One core ingredient is the MSE supported equilibrium reconstruction providing an estimation for the localization of the resonant surfaces. At ASDEX Upgrade a very generic integrated control and realtime diagnostic system has been implemented [58, 104]. This system includes any new measurement as a potential realtime diagnostic, which can announce new signals to the system. This freely programable scheme allows for an flexible application of the system for NTM control and eventually for disruption avoidance.

8. Implication and outlook for ITER

In a sequence of publications an attempt has been made to quantify the impact of NTMs and their stabilization schemes on the efficiency of energy producing tokamak, in particular for ITER [105, 106, 19]. The efficiency of an energy releasing system is defined through its gain $Q := P_{fusion}/P_{input}$. As output $P_{fusion} = 5 \cdot P_\alpha$ is taken, as the total fusion power distributed on the α-particles ($P_\alpha = 0.2 \cdot P_{fusion}$) and the neutrons ($P_n = 0.8 \cdot P_{fusion}$) according to their mass ratios. For the calculations $Q = 10$, $P_\alpha = 80MW$, $\beta_N = 1.8$ in the ITER scenario 2 [107] has been assumed. For the energy confinement τ_E without an NTM $\tau_E = H_H \cdot 3.7s$ and $H_H = 1$ has been used. $H_H = \tau_{exp}/\tau_{scaling}$ denotes the normalized energy confinement with respect to the scaling law for the confinement time for a sawtoothing ELMy H-mode. In figure 19 the resulting operation curves for constant H_H-factors in the range from 0.75 to 1.25 is shown as function of the additionally applied ECCD power and the Q-factor.

At the onset the discharge sits on the curve with $H_H = 1$ without any additional ECCD power applied. After the NTM-onset Q and H_H drop significantly down to $Q(3/2) = 6.9$ and $Q(2/1) = 4.7$ and to $H_H(3/2) = 0.85$ and $H_H(2/1) = 0.75$ for a (3/2) and (2/1)-NTM respectively (points A and B in figure 19). If the (2/1)-NTM locks the situation becomes worse and $H_H(2/1)$ becomes even lower. Applying now additional 20 MW ECCD power for the removal of the corresponding modes, one gets back to full energy confinement time τ_E, i.e. $H_H = 1$, but now at lower Q-values. The additional ECCD power has to be included in the energy balance. For 20 MW one arrives at $Q \approx 7$, for the optimistic case with only 10 MW needed, one arrives at $Q \approx 8.5$. Once the NTM has been stabilized, one can arrive along the $H_H = 1$ curve again towards $Q = 10$, by switching off the gyrotrons. When the next NTM

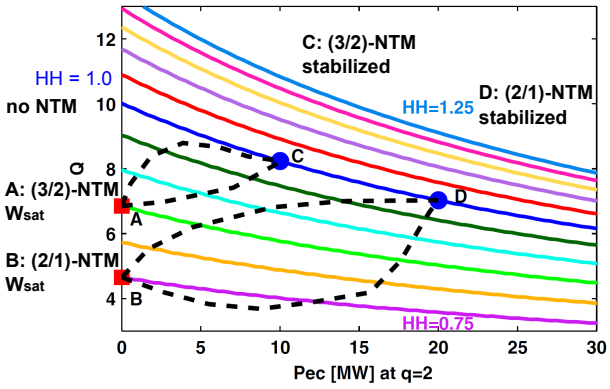

Figure 19. Energy gain Q as function of the additionally required ECCD power for a complete or partial removal of an existing NTM (figure 1 taken from [19]). The curves indicate the operational points for a fixed H_H-factor in the range $H_H = 0.75...1.25$ in steps of 0.05.

gets triggered, this loop is followed again and the gyrotrons are applied.

An incomplete stabilization of the NTM with only a partial confinement recovery, i.e. only a reduction in the island size, will result in a working point in the range between the broken curves. Triggering the FIR-regime would also be in this area of the diagram. A continuously applied preemptive ECCD will reduce the achievable Q-value, correspondingly.

In ITER such a control scheme will have to be an integral part of the control system. This part will mainly be responsible for the steering of the mirrors and the deposited power from the connected gyrotrons. The low field side equatorial launcher (EL) is optimized for central heating and current drive in a radial range of $\rho_{pol} \approx 0...0.5$, whereas the upper launcher (UL) is optimized for $\rho_{pol} \approx 0.3...0.9$. The upper launcher is primarily designed for the purpose of (3/2) and (2/1)-NTM control and sawtooth tailoring. It consists of two different designs for a set of upper steering mirrors (USM) and a set of lower steering mirrors (LSM). An comprehensive overview over the present design is given in [108]. The system has been optimized for a narrow deposition (target: $2d_{dep} < W_{marg}$) with a maximization of $\eta_{NTM} = j_{cd}/j_{bs}$, in order to avoid the need for a modulation of the gyrotrons. The gyrotrons provide an total power of 20 MW at 170 MHz. These optimizations are a partially ongoing process driven by new experimental and theoretical input.

From the combined ASDEX Upgrade and JT-60U data the following predictions for the required ECCD power and alignment have been made [24]. For the ITER scenario 2 [107] and a deposition width of 3-4 cm with prefect alignment onto the resonant surface, an estimation for the required ECCD power for an unmodulated and a modulated case has been given. For the (3/2)-NTM 10 MW and 7 MW, for the (2/1)-NTM 10 MW and 9 MW are predicted for a complete stabilization. A possible misalignment is expressed in terms of the deposition width $x_{mis}/(2d_{dep})$. With the presently planed 20 MW of ECCD power, for the (3/2)-NTM a misalignment of $x_{mis}(3/2, unmod.)/(2d_{dep}) = 0.4$ for the unmodulated case, and $x_{mis}(3/2, mod.)/d_{dep} = 0.6$ for the modulated case is possible while still stabilizing the mode. For the (2/1)-NTM $x_{mis}(2.1, unmod.)/(2d_{dep}) = 0.5$ and $x_{mis}(2/1, mod.)/(2d_{dep}) = 0.8$ has been estimated. From this considerations, the ECCD system should be able to fulfill its

purpose.

In the more recent analytical approach for η_{NTM} also the ITER scenario 2 has been used as reference [31]. A different criterion for the ECCD system has been derived

$$2d_{dep} \leq 5 \text{ cm}, \qquad \text{and} \qquad (2d_{dep}) \cdot \eta_{NTM} \geq 5 \text{ cm}. \tag{3}$$

Calculating with these constraints with the TORBEAM raytracing code the resulting needs on the mirror system, a modification of the steering capability towards a larger toroidal launching angle is suggested. These modifications should result in a reduction of the the needed ECCD power of 25% for the lower steering mirror and 10% for the upper steering mirror.

The discussion on details of the ECCD system, in particular the upper launcher is still a field were new input might require some modifications. A design change however, should be based only on the most reliably understood theoretical consideration and experimentally verified information.

9. Summary and conclusions

In this publication an attempt has been made to summarize the present status of experiments on NTM control. This consists of two approaches, namely the avoidance of NTMs at all, and the stabilization or mitigation of unavoidable NTMs. For the avoidance different schemes of profiles tailoring (n_e, p, q-profile) and avoidance of MHD, which can trigger NTMs, have been discussed. In the improved H-mode or hybrid scenario NTMs cause only a reduced problem and the usefulness of an NTM removal there needs to be further investigated. A mitigation by attempting a transition into the FIR-regime has been indicated. For all these avoidance, stabilization or mitigation scenarios, the application of ECCD at different resonant surfaces ($q \leq 1$, $q \approx 1$ for sawtooth tailoring, $q = 4/3$ for initiating the FIR-regime, $q = 3/2$ and $q = 2$ for NTM suppression and preemptive NTM avoidance) is an appropriate tool.

As the ITER design of the ECCD and their launcher system has been driven by the ongoing work on NTM control in present devices and actual theoretical work, ITER seems to be well equipped for controlling NTMs. The available power of 20 MW at 170 GHz should be sufficient. Fine details on the upper launcher should be taken care of and possibly optimized for reduced demands on the system.

Acknowledgment

This summary has been written with a considerable amount of support and material from multiple experiments. Most of the material is based on published material and summarized here. I want to express my gratitude for the support I have received.

References

[1] SAUTER, O. et al., Phys. Rev. Lett. **88** (2002) 105001.
[2] WESTERHOF, E. et al., Nucl. Fusion **42** (2002) 1324 .
[3] SAUTER, O. et al., Phys. Plasmas **6** (1999) 2834 .

[4] SAUTER, O. et al., Plasma Phys. Controlled Fusion **44** (2002) 1999 .
[5] RUTHERFORD, R. H., Phys. Fluids **16** (1973) 1903 .
[6] FITZPATRICK, R., Phys. Plasmas **2** (1995) 825 .
[7] GLASSER, A. H. et al., Phys. Fluids **18** (1975) 875 .
[8] GLASSER, A. H. et al., Phys. Fluids **19** (1976) 567 .
[9] KOTSCHENREUTHER, M. et al., Phys. Plasmas **28** (1985) 294 .
[10] LÜTJENS, H. et al., Phys. Plasmas **8** (2001) 4267 .
[11] WILSON, H. R. et al., Phys. Plasmas **3** (1996) 248 .
[12] POLI, E. et al., Physical Review Letters **94** (2005) 205001.
[13] POLI, E. et al., Nuclear Fusion **45** (2005) 384.
[14] SICCINIO, M. et al., Physics of Plasmas **18** (2011) 122506.
[15] STOBER, J. et al., Plasma Physics and Controlled Fusion **43** (2001) A39.
[16] MARASCHEK, M. et al., Plasma Physics and Controlled Fusion **45** (2003) 1369.
[17] SAUTER, O. et al., Phys. Plasmas **4** (1997) 1654 .
[18] ZOHM, H., Phys. Plasmas **4** (1997) 3433 .
[19] SAUTER, O. et al., Plasma Phys. Controlled Fusion **52** (2010) 025002 (17pp).
[20] GÜNTER, S. et al., Nuclear Fusion **44** (2004) 524.
[21] GUDE, A. et al., Nuclear Fusion **42** (2002) 833.
[22] GÜNTER, S. et al., Physical Review Letters **87** (2001) 275001.
[23] MORRIS, A. W., Plasma Phys. Controlled Fusion **34** (1992) 1871 .
[24] URSO, L. et al., Nuclear Fusion **50** (2010) 025010 (12pp).
[25] ZOHM, H. et al., J. Phys. Conf. Ser. **25** (2005) 234.
[26] ISAYAMA, A. et al., Nucl. Fusion **49** (2009) 055006 (9pp).
[27] PETTY, C. C. et al., Nucl. Fusion **44** (2004) 243 .
[28] HAYE, R. L. et al., Nucl. Fusion **46** (2006) 451 .
[29] ZOHM, H. et al., Plasma Physics and Controlled Fusion **49** (2007) B341.
[30] ISAYAMA, A. and the JT60 Team, Nucl. Fusion **47** (2007) 773 .
[31] BERTELLI, N. et al., Nucl. Fusion **51** (2011) 103007 (15pp).
[32] MARASCHEK, M. et al., Physical Review Letters **98** (2007) 025005.
[33] POLI, E. et al., Physics of Plasmas **6** (1999) 5.
[34] POLI, E. et al., Computer Phys. Comm. **136** (2001) 90 .
[35] POLI, E. et al., Fusion Eng. Design **53** (2001) 9 .
[36] MATSUDA, K., IEEE Trans. Plasma Scien. **17** (1989) 6 .
[37] ISAYAMA, A. et al., Plasma Phys. Controlled Fusion **42** (2000) L37 .
[38] ISAYAMA, A. et al., Nucl. Fusion **43** (2003) 1272 .
[39] HEGNA, C. C. et al., Phys. Plasmas **4** (1997) 2940 .
[40] VOLPE, F. A. G. et al., Phys. Plasmas **16** (2009) 102502.
[41] KOSHURIINOV, Y. I. et al., Technical Physics Letters **31** (2005) 709 .
[42] BONGERS, W. A. et al., ECE system on ASDEX-Upgrade placed inline at the high power waveguide based transmission system, in *2009 34TH INTERNATIONAL CONFERENCE ON INFRARED, MILLIMETER, AND TERAHERTZ WAVES*, pages 590–591, 2009.
[43] ERCKMANN, V. et al., Fusion Science and Technology **55** (2009) 23 .
[44] WESTERHOF, E., FOM Institute DIFFER (Dutch Institute for Fundamental Energy Research), private communication (2011).
[45] GRAVES, J. P. et al., Phys. Rev. Lett. **102** (2009) 065005.
[46] GRAVES, J. P. et al., Nucl. Fusion **50** (2010) 052002 (6pp).
[47] WARRICK, C. D. et al., Phys. Rev. Lett. **85** (2001) 574 .
[48] WARRICK, C. D. et al., NEO-CLASSICAL TEARING MODE STABILISATION AND ONSET MECHANISMS IN COMPASS-D, in *Europhysics Conference Abstracts (CD-ROM, Proc. of the 28th EPS Conference on Controlled Fusion and Plasma Physics, Madeira 2001)*, edited by SILVA, C. et al., volume 25A, pages 1817–1820, Geneva, 2001, EPS.

[49] EVANS, T. E. et al., Phys. Rev. Lett. **92** (2004) 235003.

[50] SUTTROP, W. et al., Design of in-vessel saddle coils for MHD control in ASDEX Upgrade, in *Europhysics Conference Abstracts (CD-ROM, Proc. of the 35th EPS Conference on Plasma Physics, Hersonissos, Crete, 2008)*, edited by LALOUSIS, P. and MOUSTAIZIS, S., volume 32D, pages P–4.075, Geneva, 2008, EPS.

[51] SUTTROP, W. et al., Fusion Engineering and Design **84** (2009) 290.

[52] SUTTROP, W. et al., Phys. Rev. Lett. **106** (2011) 225004.

[53] CIRRANT, S. et al., Mode Coupling Trigger of Tearing Modes in ECW Heated Discharges in FTU, in *Fusion Energy 2000 (Proc. 18th Int. Conf., Sorrento, Italy, 2000)*, volume IAEA-CSP-8/C, CD-ROM file EX/3-3 and http://www-pub.iaea.org/MTCD/publications/PDF/csp_008c/html/node1.htm, (Vienna: IAEA).

[54] HICKS, N. et al., Fusion Science and Technology **57** (2010) 1.

[55] HUMPHREYS, D. A. et al., Phys. Plasmas **13** (2006) 056113 (9p).

[56] REICH, M. et al., Progress on ECCD-based NTM rt-control at ASDEX Upgrade, in *Europhysics Conference Abstracts (CD-ROM, Proc. of the 38th EPS Conference on Plasma Physics, Strasbourg, France, 2011)*, edited by MCKENNA, C., volume 34A of *ECA*, page P5.102, Geneva, 2011, European Physical Society.

[57] REICH, M. et al., Eccd-based ntm control using the asdex upgrade real-time system, in *Europhysics Conference Abstracts (CD-ROM, Proc. of the 37th EPS Conference on Plasma Physics, Dublin, Ireland, 2010)*, edited by MCKENNA, C., volume 34A of *ECA*, page P2.189, Geneva, 2010, European Physical Society.

[58] REICH, M. et al., Fusion Science and Technology **58** (2010) 727.

[59] GIANNONE, L. et al., Fusion Engineering and Design **84** (2009) 825.

[60] REICH, M. et al., Real-time current profile measurements for ntm control, in *Europhysics Conference Abstracts (CD-ROM, Proc. of the 36th EPS Conference on Plasma Physics, Sofia, Bulgaria, 2009)*, edited by MATEEV, M. and BENOVA, E., volume 33E of *ECA*, pages P–1.160, Geneva, 2009, European Physical Society.

[61] de Baar, M. R. et al., Physics and Real Time Control of Tearing modes in TEXTOR, in *Fusion Energy 2008 (Proc. 22nd Int. Conf., Geneva, Swizerland, 2008)*, volume IAEA-CN-165, CD-ROM file EX/P9-12 and http://www-naweb.iaea.org/napc/physics/FEC/FEC2008/html/index.htm, (Vienna: IAEA).

[62] HENNEN, B. A. et al., Nucl. Fusion **52** (2010) 104006.

[63] ZOHM, H. et al., Nuclear Fusion **39** (1999) 577.

[64] YU, Q. and GÜNTER, S., Modelling of the neo-classical tearing mode and its stabilisation by ECCD/ECRH, in *Europhysics Conference Abstracts (CD-ROM, Proc. of the 1998 ICPP & 25th EPS Conference on Controlled Fusion and Plasma Physics, Praha, 1998*, edited by PAVLO, P., volume 22C, pages 1899–1902, Petit-Lancy, 1998, EPS.

[65] YU, Q. and GÜNTER, S., Plasma Physics and Controlled Fusion **40** (1998) 1977.

[66] YU, Q. et al., Physics of Plasmas **7** (2000) 312.

[67] GANTENBEIN, G. et al., Physical Review Letters **85** (2000) 1242.

[68] GANTENBEIN, G. et al., Investigations on $m = 2$, $n = 1$ tearing mode stabilisation with ECRH at ASDEX Upgrade, in *Europhysics Conference Abstracts (CD-ROM, Proc. of the 30th EPS Conference on Controlled Fusion and Plasma Physics, St. Petersburg, 2003)*, edited by KOCH, R. and LEBEDEV, S., volume 27A, pages P–1.187, Geneva, 2003, EPS.

[69] ZOHM, H. et al., Plasma Physics and Controlled Fusion **39** (1997) B237.

[70] MARASCHEK, M. et al., Plasma Physics and Controlled Fusion **41** (1999) L1.

[71] ESPOSITO, B. et al., Nuclear Fusion **51** (2011) 083051.

[72] ESPOSITO, B. et al., Nuclear Fusion **49** (2009) 065014.

[73] VOLPE, F. A. G. et al., Stabilization of disruptive locked modes at DIII-D by means of ECCD and magnetic perturbations, in *15th workshop on MHD stability control: US-Japan Workshop on 3D Magnetic Field Effects in MHD Control*, page https://fusion.gat.com/conferences/mhd10/talks/Volpe_Wednesday.pdf or

https://fusion.gat.com/conferences/mhd10/talks.php, 2010.
[74] VOLPE, F. and La Haye, R. J., University of Madison (WI), USA and General Atomics, San Diego (CA), USA, private communication (2011).
[75] NAGASAKI, K. et al., Nucl. Fusion (2003) L7.
[76] NAGASAKI, K. et al., Nucl. Fusion (2005) 1608.
[77] LA HAYE, R. J. et al., Nucl. Fusion **45** (2005) L37 .
[78] PRATER, R. et al., Nucl. Fusion **47** (2007) 371 .
[79] MARASCHEK, M. et al., Scaling of the marginal β_p of neoclassical tearing modes during power ramp-down experiments in ASDEX Upgrade, in *Europhysics Conference Abstracts (CD-ROM, Proc. of the 30th EPS Conference on Controlled Fusion and Plasma Physics, St. Petersburg, 2003)*, edited by KOCH, R. and LEBEDEV, S., volume 27A, pages P–1.120, Geneva, 2003, EPS.
[80] STOBER, J. et al., Nuclear Fusion **41** (2001) 1535.
[81] ANGIONI, C. et al., Physics of Plasmas **12** (2005) 040701.
[82] MLYNEK, A. et al., Nuclear Fusion **51** (2011) 043002.
[83] ISAYAMA, A. and the JT60 Team, Phys. Plasmas **12** (2005) 056117 (10pp).
[84] SUZUKI, T. et al., Nucl. Fusion **48** (2008) 045002 (9pp).
[85] ANGIONI, C. et al., Nuclear Fusion **43** (2003) 455.
[86] ZOHM, H. et al., Nuclear Fusion **43** (2003) 1570.
[87] MÜCK, A. et al., Plasma Physics and Controlled Fusion **47** (2005) 1633.
[88] ZOHM, H. et al., Plasma Physics and Controlled Fusion **45** (2003) A163.
[89] GOODMAN, T. P. et al., Phys. Rev. Lett. **106** (2011) 245002.
[90] WITVOET, G. et al., Nucl. Fusion **51** (2011) 103043 (15pp).
[91] LAURET, M. et al., Demonstration of sawtooth period locking with power modulation in TCV plasmas, subm. to Nuclear Fusion Letters (2012).
[92] CHAPMAN, I. T. et al., Physics of Plasmas **16** (2009) 072506.
[93] IGOCHINE, V. et al., Plasma Physics and Controlled Fusion **53** (2011) 022002.
[94] CHAPMAN, I. T., Nucl. Fusion **53** (2011) 013001 (36pp).
[95] GUDE, A. et al., Nuclear Fusion **39** (1999) 127.
[96] GRUBER, O. et al., Plasma Physics and Controlled Fusion **47** (2005) B135.
[97] STÄBLER, A. et al., Nuclear Fusion **45** (2005) 617.
[98] STOBER, J. et al., Nuclear Fusion **47** (2007) 728.
[99] LUCE, T. et al., Development of advanced inductive scenarios for iter, in *Fusion Energy 2010 (Proc. 23rd Int. Conf., Daejon, Korea Rep., 2010)*, volume IAEA-CN-180, CD-ROM file ITR/1-5 and http://www-naweb.iaea.org/napc/physics/FEC/FEC2010/html/index.htm, (Vienna: IAEA).
[100] WADE, M. R. et al., Nucl. Fusion **45** (2005) 407 .
[101] PETTY, C. C. et al., Phys. Rev. Lett. **102** (2009) 045005.
[102] JOFFRIN, E. et al., Nucl. Fusion **45** (2005) 626 .
[103] SIPS, A. C. C. et al., Nuclear Fusion **47** (2007) 1485.
[104] TREUTTERER, W. et al., Fusion Engineering and Design **86** (2011) 465.
[105] SAUTER, O. and ZOHM, H., Partial stabilisation of ntms with eccd for standard scenarios in iter, in *Europhysics Conference Abstracts (CD-ROM, Proc. of the 32nd EPS Conference on Plasma Physics, Tarragona, 2005)*, edited by HIDALGO, C. and van Milligen, B. P., volume 29C, pages P–2.059, Geneva, 2005, EPS.
[106] SAUTER, O. et al., Partial stabilization and control of neoclassical tearing modes in burning plasmas, in *Fusion Energy 2006 (Proc. 21st Int. Conf., Chengdu, China, 2006)*, volume IAEA-CN-149, CD-ROM file TH/P3-10 and http://www-naweb.iaea.org/napc/physics/FEC/FEC2006/html/index.htm, (Vienna: IAEA.
[107] SHIMADA, M. et al., Progress in the ITER Physics Basis Chapter 1: Overview and summary, Nuclear Fusion **47** (2007) S1 .
[108] HENDERSON, M. et al., Nucl. Fusion **48** (2008) 054013 (14pp).